J. Fluid Mech. (2006), *vol.* 561, *pp.* 307–327.
doi:10.1017/S0022112006000802 Printed in the United Kingdom

Similarity solutions for fluid injection into confined aquifers

By JAN M. NORDBOTTEN[1,2] AND MICHAEL A. CELIA[2]

[1]Department of Mathematics, University of Bergen, Joh. Brunsgate 12, 5008 Bergen, Norway
[2]Civil and Environmental Engineering, Princeton University, Princeton, NJ 08544, USA

(Received 19 February 2005 and in revised form 20 January 2006)

Fluid injection into the deep subsurface, such as injection of carbon dioxide (CO_2) into deep saline aquifers, often involves two-fluid flow in confined geological formations. Similarity solutions may be derived for these problems by assuming that a sharp interface separates the two fluids, by imposing a suitable no-flow condition along both the top and bottom boundaries, and by including an explicit solution for the pressure distribution in both fluids. When the injected fluid is less dense and less viscous than the resident fluid, as is the case for CO_2 injection into a resident brine, gravity override produces a fluid flow system that is captured well by the similarity solutions. The similarity solutions may be extended to include slight miscibility between the two fluids, as well as compressibility in both of the fluid phases. The solutions provide the location of the interface between the two fluids, as well as drying fronts that develop within the injected fluid. Applications to cases of supercritical CO_2 injection into deep saline aquifers demonstrate the utility of the solutions, and comparisons to solutions from full numerical simulations show the ability to predict the system behaviour.

1. Introduction

Fluids are injected into confined porous media around the world for the purposes of enhanced oil recovery, gas storage and waste disposal (see, for example, Donaldson 1964; US Environmental Protection Agency 1985; Smith 1996; Bachu & Gunter 2004). When the injected fluid is immiscible with the resident fluid(s), a multi-phase flow problem results with no inter-phase mass transfer. When the injected fluid is slightly miscible with the resident fluid, then mass transfer between fluids may need to be included in the analysis. In this paper, we consider injection into a porous formation that is confined above and below by impervious caprock formations, with slight miscibility between the injected fluid and the resident fluid. We show that the interface between the injected fluid and the resident fluid, as well as the drying front associated with residual fluid evaporating into the injected fluid, has an asymptotic solution in the form of a self-similar shape.

There are many solutions for interface propagation in the literature that are based on self-similarity. These include the pioneering work of Barenblatt and co-workers (see Barenblatt 1990; Barenblatt 1996 and references therein), and, among many others, the work of Woods and co-workers that includes multiple layers (Huppert & Woods 1995; Woods & Mason 2000; King & Woods 2003) and reaction fronts (Raw & Woods 2003; Jupp & Woods 2003). While these solutions are elegant and have significant practical applications, they are derived for systems with incompressible fluids, and

almost always applied to unconfined formations. In the current work, we consider the case of continuous injection into a confined formation. Our overall solution includes mass transfer between the two fluids, and allows for fluid compressibilities to be included in the solution.

As a practical application of this model, we consider injection of carbon dioxide (CO_2) into deep saline aquifers. This has been proposed as a means of reducing anthropogenic emissions of CO_2 into the atmosphere (e.g. Bruant *et al.* 2002). Several commercial-scale operations are already active (for example, Torp & Gale 2004; Holloway *et al.* 2004), although thousands more are required to make an impact on global warming (Pacala & Socolow 2004). For efficiency of storage, CO_2 will typically be injected as a supercritical fluid (that is, in conditions where pressure and temperature both exceed their critical values), thereby requiring injection depths greater than about 800 m. At these conditions, CO_2 remains less dense and less viscous than the resident brine (Bachu 2003), thus we expect the injection profile to show significant gravity override (Nordbotten *et al.* 2005*b*). Further, as CO_2 displaces brine, some of the brine is left behind in immobile pockets, resulting in a so-called residual saturation of the brine, where saturation is defined as the fraction of void space filled with brine, and the term 'residual' implies that the brine is immobile. We expect to see residual brine and CO_2 equilibrate behind the CO_2–brine interface owing to the slight solubility of CO_2 in water (Enick & Klara 1990). Because CO_2 is typically injected as a dry phase, some of the residual brine will evaporate into the dry CO_2, forming an invading CO_2 front that is saturated with water (we refer to this as wet CO_2). The evaporation of the residual water eventually leads to the formation and propagation of a drying front behind the main CO_2 invasion front, where behind the drying front no water is present.

Our model will apply to injection into a planar, horizontally homogeneous confined aquifer. We will make vertical equilibrium assumptions and seek to reduce the system of governing partial differential equations to a system of ordinary differential equations in a single similarity variable. We present the solution as a series of increasingly complex problems, beginning with the incompressible and non-reactive case, then including reaction, and finally including full fluid compressibility. Example calculations are used to demonstrate the behaviour of the solution, and include comparisons to full numerical solutions of the modelled systems.

2. Problem statement

The problem of interest is injection of an invading fluid, such as carbon dioxide, into a confined subsurface formation that contains a different resident fluid, such as brine. The injected fluid will move radially outward from the well. Because of density differences between the two fluids, gravity override will occur. If the injected fluid is less viscous than the ambient fluid, viscous instability will combine with gravity override to enhance the invasion of injected fluid along the top of the formation. For cases of viscous domination, the system is described well by the solution of the radial Buckley–Leverett equation, subject to buoyant segregation of the fluids, which was shown in Nordbotten *et al.* (2005*b*). In that paper, a simplified solution was derived based on minimum energy principles, for the case when buoyancy acts to segregate the fluids, but does not otherwise play a significant role. The result was an equation like that given by (14) in the present paper. That solution is a simple case of the more general solution derived herein. The work of Nordbotten *et al.* (2005*b*) also proposed a heuristic solution for the case when buoyancy is more dominant, but the basis of

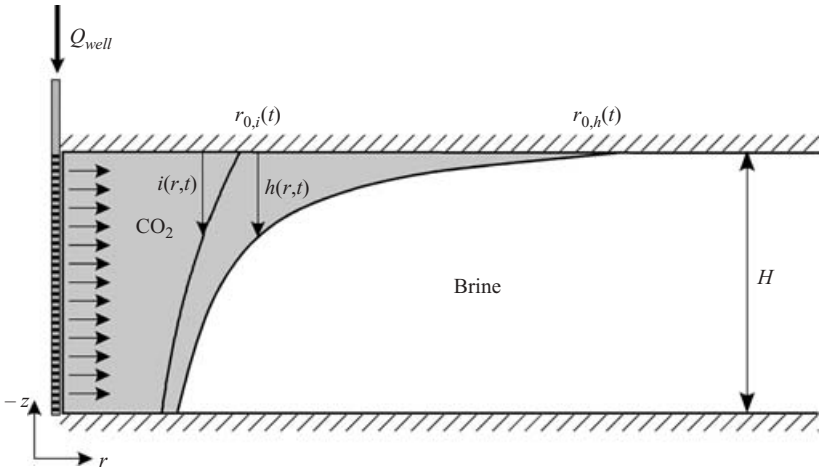

FIGURE 1. Schematic diagram showing a typical plume of injected fluid of thickness $h(r, t)$ trailed by a drying front denoted by $i(r, t)$. The outer extents of $h(r, t)$ and $i(r, t)$ are denoted $r_{0,h}(t)$ and $r_{0,i}(t)$.

that argument was not well constructed, and the present development is much more rigorous and general in its development. When buoyancy becomes important, the simple Buckley–Leverett solution in Nordbotten *et al.* (2005*b*) is no longer adequate, and a more general approach must be used.

In the present work, we allow for strong buoyant drive, within an aquifer of height H that is confined both above and below. We will further allow for miscibility of the fluids, which is consistent with the behaviour of CO_2 and brine. We will also allow for pressure dependence of fluid densities and viscosities. We ignore capillary pressure effects in the solution. Under these conditions, the injected fluid, which we take to be CO_2, forms an invasion front in the (r, z)-plane, with its thickness denoted by $h(r, t)$ (with units [L]), as shown in figure 1. Behind this front resides invading CO_2 along with whatever residual brine saturation exists after the invasion. Because we allow for equilibrium mass transfer between the two fluid phases (thus modelling phase partitions as instantaneous), the residual brine will be saturated with dissolved CO_2. In addition, the CO_2 will be saturated with water vapour. However, because the injected CO_2 is assumed to be dry, there will be a drying front that forms behind the CO_2 invasion front. Behind the drying front, all residual water has been evaporated in the invading CO_2. This drying front is denoted by $i(r, t)$ [L] in figure 1. The problem at hand is to derive solutions for $h(r, t)$ and $i(r, t)$, given a constant injection rate Q_{well} [L^3T^{-1}] of CO_2 into a confined formation of thickness H [L].

3. General theory and solution

We will present the similarity solutions in three progressively complex cases. This approach has been chosen to make the presentation as accessible as possible, since the equations involved and the derivation is much clearer for the less complex cases. In the following two sections, we will first present the case of no mass transfer and incompressible fluids, followed by the extension to include mass transfer between the brine and the CO_2. The full formulation including compressibility is included in Appendix C.

3.1. *No mass transfer, incompressible fluids*

To demonstrate the basic approach that accounts for confined aquifer conditions, we first solve the simplest case associated with figure 1, which is the case for fully immiscible and incompressible fluids. This case is analogous to the one described in Huppert & Woods (1995), with the modifications that viscosity ratios not equal to unity are included, and the formulation is in axisymetric coordinates. In this case the only front in figure 1 is $h(r,t)$, and all fluid properties are assumed to be constant. The CO_2 region just behind the invasion front $h(r,t)$ has residual amounts of brine saturation left behind. Let the fraction of pore space filled with residual brine be denoted by $S_{res}[L^0]$. Typical values of S_{res} are between 5 and 20 % (Dullien 1992). We will approximate the residual saturation to be constant behind the invading front. Let the vertical coordinate z be defined as positive downward, and assume the system is radially symmetric about an injection well from which CO_2 is injected at a constant rate into a brine-filled confined aquifer. We begin by writing the following equation to describe the vertical variability of pressure for any given (r,t):

$$p(r,t,0) = p(r,t,H) - \int_0^{h(r,t)} \left[\rho_c g + \frac{q_{c,z}(r,t,z)\mu_c}{k_z k_{r,c}}\right] \mathrm{d}z - \int_{h(r,t)}^{H} \left[\rho_w g + \frac{q_{w,z}(r,t,z)\mu_w}{k_z k_{r,w}}\right] \mathrm{d}z. \tag{1}$$

In (1), subscripts c and w refer to CO_2 and water, respectively. Density of fluid α ($\alpha = c, w$) is denoted by ρ_α [ML^{-3}], g is the gravitational constant [LT^{-2}], $q_{\alpha,z}$ is the z-component of the volumetric flux vector [LT^{-1}], μ_α denotes the dynamic viscosity of fluid α [$M\ L^{-1}T^{-1}$], k_z is the permeability in the z direction [L^2], and $k_{r,\alpha}$ is the relative permeability of the porous medium to fluid $\alpha[L^0]$. Darcy's law has been used to account for potential losses due to vertical flows. When the contribution to the pressure variation in (1) from the flux terms is negligible, we can use the assumption of vertical equilibrium. This is appropriate for systems in which the vertical length scale is much smaller than the horizontal length scale (Huppert & Woods 1995; see also Appendix D of this paper). Vertical equilibrium allows (1) to be simplified as

$$p(r,t,0) = p(r,t,H) - (H - h(r,t))\rho_w g - h(r,t)\rho_c g. \tag{2}$$

Equation (2) implies that knowledge of pressure at any point along z provides pressures at all values of $0 \leqslant z \leqslant H$.

Next the vertically integrated volume balance equation for each fluid is written for this radial system. The approach follows standard vertical averaging as used in aquifer descriptions, and as described in standard groundwater hydrology textbooks such as Bear (1979). For example, the equation for the brine (equation (3*b*) below) follows directly from the vertical integration of the point mass-balance equation, with an assumption of essentially horizontal flow and radial symmetry. The resulting set of equations for the CO_2 and the brine may be written as:

$$-\frac{\partial h}{\partial t} = \frac{1}{2\pi\varphi(1 - S_{res})} \frac{1}{r} \frac{\partial Q_c}{\partial r}, \tag{3a}$$

$$-\frac{\partial (H - h)}{\partial t} = \frac{1}{2\pi\varphi(1 - S_{res})} \frac{1}{r} \frac{\partial Q_w}{\partial r}, \tag{3b}$$

where ϕ denotes porosity [L^0], S_{res} denotes residual saturation of the resident brine, and the radially dependent vertically integrated flow rates Q_α are defined by

$$Q_c = -2\pi r h k \frac{k_{r,c}}{\mu_c} \frac{\partial p_c}{\partial r}, \tag{4a}$$

$$Q_w = -2\pi r (H-h) k \frac{k_{r,w}}{\mu_w} \frac{\partial p_w}{\partial r}. \tag{4b}$$

In (4*a*, *b*), p_α is the pressure in fluid α[$ML^{-1}T^{-2}$], and k denotes the permeability in the horizontal direction [L^2]. Note that the term $\varphi(1-S_{res})$ in (3*a*, *b*) corresponds to the 'specific yield' or 'drainable porosity' term that arises in groundwater hydrology (Bear 1979, pp. 88, 99, 114). This term may be seen as a measure of the amount of pore space that is invaded by CO_2 as the front moves into the brine region of the domain. Substitution of (2) and (4) into (3), and summation of (3*a*) and (3*b*), lead to the following equation

$$0 = \frac{k}{\varphi(1-S_{res})r}\left[\frac{\partial}{\partial r}\left(\lambda_c h r \frac{\partial}{\partial r}(p - \Delta\rho g h)\right) + \frac{\partial}{\partial r}\left(\lambda_w (H-h) r \frac{\partial p}{\partial r}\right)\right], \tag{5}$$

where the pressure p, without any subscript, is defined as the pressure at the bottom of the aquifer, that is, $p \equiv p(r, t, H)$. In (5), we have defined the phase mobility as $\lambda_\alpha = k_{r,\alpha}/\mu_\alpha$[$LTM^{-1}$]. Integration of (5) implies that

$$C = \lambda_c h r \frac{\partial}{\partial r}(p - \Delta\rho g h) + \lambda_w (H-h) r \frac{\partial p}{\partial r}. \tag{6}$$

The constant of integration in (6), C, is evaluated by the condition that CO_2 is injected at a fixed rate given by Q_{well}. This condition implies that $C = -Q_{well}/2\pi k$.

Substitution for the integration constant in (6) and rearrangement allows the pressure derivative to be written as

$$\frac{\partial p}{\partial r} = [\lambda_c h + \lambda_w (H-h)]^{-1}\left[\lambda_c h \frac{\partial}{\partial r}(\Delta\rho g h) - \frac{Q_{well}}{2\pi r k}\right]. \tag{7}$$

The equation allows the confined pressure to be represented in the system. When (7) is substituted into (3*a*), with appropriate substitutions for the flow and pressure terms in the equation, an equation for the unknown interface location, $h(r, t)$, may be written,

$$\frac{\partial h}{\partial t} = \frac{\Delta\rho g k \lambda_w}{\varphi(1-S_{res})r}\frac{\partial}{\partial r}\left[\frac{\lambda_c h(H-h)r}{\lambda_c h + \lambda_w (H-h)}\frac{\partial h}{\partial r} + \frac{Q_{well}(H-h)}{2\pi(\lambda_c h + \lambda_w (H-h))}\frac{1}{\Delta\rho g k}\right]. \tag{8}$$

More generally, we may define the following dimensionless groupings associated with (8),

$$\left.\begin{aligned} \Gamma &\equiv \frac{2\pi\Delta\rho g k \lambda_w H^2}{Q_{well}}, \quad \lambda \equiv \frac{\lambda_c}{\lambda_w}, \\ \tau &\equiv \frac{Q_{well} t}{2\pi H \varphi K (1-S_{res})}, \quad \eta \equiv \frac{r}{\sqrt{k}}, \quad h' \equiv \frac{h}{H}. \end{aligned}\right\} \tag{9}$$

Use of these groups simplifies (8) to the following,

$$\frac{\partial h'}{\partial \tau} = \frac{1}{\eta}\frac{\partial}{\partial \eta}\left[\frac{\Gamma\lambda h'(1-h')\eta}{\lambda h' + (1-h')}\frac{\partial h'}{\partial \eta} + \frac{1-h'}{\lambda h' + (1-h')}\right], \tag{10}$$

where $h' = h'(\eta, \tau)$. Finally, (10) may be rewritten using the scaling variable $\chi \equiv \eta^2/\tau$ to yield the following second-order differential equation in dimensionless form,

$$\tau\frac{\partial h'}{\partial \tau} - \chi\frac{\partial h'}{\partial \chi} = 2\frac{\partial}{\partial \chi}\left[\frac{1-h'}{1+(\lambda-1)h'}\left(2\Gamma\lambda\chi h'\frac{\partial h'}{\partial \chi} + 1\right)\right]. \tag{11}$$

In (11), the dependent variable is now interpreted as $h' = h'(\chi, \tau)$. By expanding the term in square brackets and dividing through by $\mathrm{d}h'/\mathrm{d}\chi$, (11) can be written as a partial differential equation of the following form,

$$\begin{aligned}\tau\frac{\partial h'}{\partial \tau}\left(\frac{\partial h'}{\partial \chi}\right)^{-1} = \chi - \left[1 + \Gamma\lambda\chi\frac{\partial (h')^2}{\partial \chi}\right]\frac{2\lambda}{(1+(\lambda-1)h')^2} \\ + 4\Gamma\lambda\frac{1-h'}{1+(\lambda-1)h'}\left(h' + \chi\frac{\partial h'}{\partial \chi} + h'\chi\frac{\partial^2 h'}{\partial \chi^2}\left(\frac{\partial h'}{\partial \chi}\right)^{-1}\right),\end{aligned} \tag{12}$$

where the condition that $\mathrm{d}h'/\mathrm{d}\chi \neq 0$ has been used. The time-dependent equation (12) has the stationary solution (which is proved to be stable for small Γ in Appendix A), which is a self-similar solution of the original problem (Barenblatt 1996) satisfying the nonlinear second-order ordinary differential equation,

$$\begin{aligned}0 = \chi - \left[1 + \Gamma\lambda\chi\frac{\mathrm{d}(h')^2}{\mathrm{d}\chi}\right]\frac{2\lambda}{(1+(\lambda-1)h')^2} + 4\Gamma\lambda\frac{1-h'}{1+(\lambda-1)h'} \\ \times\left(h' + \chi\frac{\mathrm{d}h'}{\mathrm{d}\chi} + h'\chi\frac{\mathrm{d}^2 h'}{\mathrm{d}\chi^2}\left(\frac{\mathrm{d}h'}{\mathrm{d}\chi}\right)^{-1}\right) \quad \text{when} \quad \frac{\partial h'}{\partial \chi} \neq 0.\end{aligned} \tag{13}$$

This equation is analogous to the radial Buckley–Leverett equation given as (16) in Blunt & King (1991). This analogy follows from interpreting saturation and capillary pressure in their formulation as plume thickness and pressure difference from the top to the bottom of the formation in our formulation.

We immediately see that for cases where the dimensionless grouping Γ, associated with gravity, is negligibly small, (13) reduces to an algebraic expression which can be inverted to give $h'(\chi)$:

$$h' = \begin{cases} 1 & \text{for} \quad \chi \leqslant 2/\lambda, \\ \dfrac{1}{(\lambda-1)}\left(\sqrt{\dfrac{2\lambda}{\chi}} - 1\right) & \text{for} \quad 2/\lambda < \chi < 2\lambda, \\ 0 & \text{for} \quad \chi \geqslant 2\lambda. \end{cases} \tag{14}$$

Equation (14) is the result derived by Nordbotten *et al.* (2005*b*), using arguments of energy minimization and an *a priori* assumption that Γ is negligibly small. Note that (14) is valid for all $\lambda \geqslant 1$. In the limit as λ goes to 1, (14) yields a solution that approaches a piecewise constant, corresponding to piston-like displacement in the formation. For values of λ less than 1, (14) does not capture the physical solution, because it has an inherent assumption of gravity override in the shape of the front. For the case of $\lambda < 1$, we use the solution of (13) that is the degenerate case of $\mathrm{d}h'/\mathrm{d}\chi = 0$, which means that the solution h' is a piecewise constant function. This again corresponds to the case of piston-like displacement.

Solution of (13) when Γ is not negligible requires specification of appropriate boundary conditions. The first is that there exists a finite innermost location where $h=0$, denoted by $r_{0,h}$. The second condition is that the solution must satisfy the volume balance

$$\int_0^{r_{0,h}} \varphi(1-S_{res})h(r,t)2\pi r\mathrm{d}r = Q_{well}t, \tag{15}$$

where $Q_{well}t$ is the cumulative injected volume of CO_2, and the integral represents the volume constrained by $h(r,t)$. This condition may be restated in dimensionless form as

$$\int_0^{\chi_{0,h}} h'(\chi)\mathrm{d}\chi = 2, \tag{16}$$

where $\chi_{0,h}$ is equal to $\eta_{0,h}(r_{0,h}(t))^2/\tau(t)$. The set of equations (13) and (16) may be solved numerically for $h'(\chi)$, by choosing an initial guess for $\chi_{0,h}$ (e.g. by using the explicit solution obtained for $\Gamma=0$), solving (13), and updating $\chi_{0,h}$ iteratively to satisfy (16). Notice that the constraint of (16) also allows the piecewise constant solutions of (13) for the case of $\Gamma=0$ and $\lambda\leqslant 1$ to be determined explicitly as

$$h' = \begin{cases} 0 & \text{for} \quad \chi < 2, \\ 1 & \text{for} \quad \chi > 2, \end{cases}$$

where the discontinuity is chosen to satisfy the mass balance requirement of (16).

Once $h'(\chi)$ is determined, the variation in the pressure field may be calculated based on (7), which may be rewritten in dimensionless variables as

$$-\frac{\mathrm{d}p'}{\mathrm{d}\chi} = \frac{1}{h'(\lambda-1)+1}\left[h'\lambda\frac{\mathrm{d}h'}{\mathrm{d}\chi} + \frac{1}{2\Gamma\chi}\right], \tag{17}$$

where $p' \equiv p/\Delta\rho g H$. For an incompressible system in an infinite domain, the pressure becomes unbounded as χ goes to 0 and infinity. For systems that are slightly compressible, we can apply finite outer boundary conditions to the pressure equation (17) by a limit condition at large radial distances χ_∞ imposed as $p(\chi_\infty)=p_0$. The outer boundary, moving as $r_\infty^2(t)=Bt$, with B a constant, is consistent with representation of slight compressibility of the porous medium (Nordbotten *et al.* 2004, 2005*b*), and is consistent with approaches such as the Cooper–Jacob expansion for well testing (see discussion in Nordbotten *et al.* 2004).

3.2. *Extension to include mass transfer and drying fronts*

In this case, we assume that CO_2 partitions into the brine, with the volume fraction of CO_2 in the residual brine denoted by β_1 [L^0]. Furthermore, assume the brine (water) can evaporate into the CO_2 phase, with the volume fraction of water vapour in the CO_2 phase denoted by β_2 [L^0]. Both of these fractions are small, of the order of a few per cent (Enick & Klara 1990). We assume the injected fluid is dry CO_2, with no water vapour. Therefore the injected CO_2 can evaporate the residual water, eventually leading to a drying front, which is denoted by $i(r,t)$ in figure 1. Between the fronts $i(r,t)$ and $h(r,t)$ exists a region of residual CO_2-saturated brine and 'wet' CO_2, while behind the front $i(r,t)$ is only dry CO_2.

The procedure to derive expressions for the two fronts is analogous to that presented in the previous section, except now we have two fronts and three flow regions. Define the radially dependent vertically integrated volumetric flow rates for the three fluids as Q_w, Q_c and Q_{cw}, where subscript w denotes water, c denotes dry CO_2, and cw

denotes wet CO_2. Mass conservation for each fluid may be written as

$$-2\pi r\varphi\frac{\partial(H-h)}{\partial t} = \frac{\gamma_1}{1-S_{res}}\frac{\partial Q_w}{\partial r}, \tag{18a}$$

$$-2\pi r\varphi\frac{\partial i}{\partial t} = \frac{\gamma_2}{1-S_{res}}\frac{\partial Q_c}{\partial r}, \tag{18b}$$

$$Q_{cw} + Q_c + Q_w = Q_{well}. \tag{18c}$$

Equation (18*c*) expresses the vertically integrated statement of divergence-free flows, which follows from the incompressibility of the system. In (18*a*) and (18*b*), the factor $(1-S_{res})$ accounts for the change in saturation across the front $h(r,t)$, while the factors γ_1 and γ_2 take account of mass exchange between brine and CO_2. The dimensionless factors γ_1 and γ_2 are derived in Appendix B, and take the forms

$$\gamma_1 = \left[1+\frac{\beta_1 S_{res}}{(1-S_{res})(1-\beta_2)}\right]^{-1}, \quad \gamma_2 = \left[1+\frac{(1-\beta_1)S_{res}}{(1-S_{res})\beta_2}\right]^{-1},$$

where β_1 and β_2 are as defined previously. The vertically integrated flow rates Q_α in (18) are defined by

$$Q_c = -2\pi r i k\frac{k_{r,c}}{\mu_c}\frac{\partial p_c}{\partial r}, \tag{19a}$$

$$Q_{cw} = -2\pi r(h-i)k\frac{k_{r,cw}}{\mu_{cw}}\frac{\partial p_{cw}}{\partial r}, \tag{19b}$$

$$Q_w = -2\pi r(H-h)k\frac{k_{r,w}}{\mu_w}\frac{\partial p_w}{\partial r}. \tag{19c}$$

The form of these equations may be derived by simple extension of (3) and (4). In particular, the right-hand side of Equation (18*a*) is modified by the factor γ_1, as compared to (3*a*), because now the volume fraction that is relevant corresponds to the amount of pore space invaded by wet CO_2, modified by the fact that some of the invading CO_2 partitions into the newly formed residual brine behind the front $h(r,t)$. Similar arguments apply to the other terms in the set of vertically–averaged mass balance equations.

For this case, the vertical equilibrium assumption (2) gives us the relationships

$$\frac{\partial}{\partial r}p_{cw} = \frac{\partial}{\partial r}(p_w + (\rho_w-\rho_{cw})gh), \quad \frac{\partial}{\partial r}p_c = \frac{\partial}{\partial r}(p_w + (\rho_w-\rho_{cw})gh + (\rho_{cw}-\rho_c)gi).$$

Inserting (19*a–c*) into (18*a–c*) and using the vertical equilibrium assumption leads to

$$\frac{\mathrm{d}}{\mathrm{d}\chi}h' = \frac{4\Gamma\gamma_1}{\chi}\frac{\mathrm{d}}{\mathrm{d}\chi}\left((1-h')\chi\frac{\mathrm{d}}{\mathrm{d}\chi}p'\right), \tag{20a}$$

$$-\frac{\mathrm{d}}{\mathrm{d}\chi}i' = \frac{4\gamma_2\Gamma\lambda_1}{\chi}\frac{\mathrm{d}}{\mathrm{d}\chi}\left(i'\chi\frac{\mathrm{d}}{\mathrm{d}\chi}(p'+h'+\vartheta i')\right), \tag{20b}$$

$$\frac{\mathrm{d}}{\mathrm{d}\chi}p' = -\frac{\dfrac{1}{2\Gamma\chi}+(\lambda_2 h'+(\lambda_1-\lambda_2)i'))\dfrac{\mathrm{d}}{\mathrm{d}\chi}h'+\lambda_1 i'\vartheta\dfrac{\mathrm{d}}{\mathrm{d}\chi}i'}{\lambda_2(h'-i')+\lambda_1 i+(1-h')}, \tag{20c}$$

where the new dimensionless groupings are defined as

$$\lambda_1 = \frac{\lambda_c}{\lambda_w}, \quad \lambda_2 = \frac{\lambda_{cw}}{\lambda_w}, \quad \vartheta = \frac{\rho_{cw}-\rho_c}{\rho_w-\rho_{cw}}. \tag{21}$$

Note that p' and Γ are defined in terms of the difference in density between the water and wet CO_2:

$$p' = \frac{p}{(\rho_w - \rho_{cw})gH}, \quad \Gamma \equiv \frac{2\pi(\rho_w - \rho_{cw})gk\lambda_w H^2}{Q_{well}}, \tag{22}$$

and the volume balance equation (16) must be modified so that it correctly accounts for the phase partitioning;

$$\int_0^{\chi_{0,h}} h'(\chi)\,\mathrm{d}\chi = 2\gamma_1. \tag{23}$$

Two additional conditions are required to solve for the interface $i' \equiv i/H$ in (20*b*). The first is that there exists a finite innermost location where $i' = 0$, denoted by $\chi_{0,i}$. The second condition is a volume balance equation analogous to (23);

$$\int_0^{\chi_{0,i}} i'(\chi)\,\mathrm{d}\chi = \frac{\gamma_2}{\gamma_1}\int_0^{\chi_{0,h}} h'(\chi)\,\mathrm{d}\chi = 2\gamma_2. \tag{24}$$

We see that (20*c*) can be used to eliminate $\mathrm{d}p'/\mathrm{d}\chi$ in (20*a*) and (20*b*), such that only two of equations (20) are coupled. These equations must be solved numerically, leading to solutions for both the initial invasion front and the drying front.

With assumptions that wet and dry CO_2 have the same density and mobility, the pressure equation (20*c*) simplifies, and (20*a*) and (20*b*) can be rewritten as a set of decoupled ordinary differential equations given by

$$\frac{\mathrm{d}h'}{\mathrm{d}\chi} = 2\gamma_1\chi^{-1}\frac{\mathrm{d}}{\mathrm{d}\chi}\left[\frac{h'-1}{h'(\lambda-1)+1}\left(2\Gamma\lambda h'\chi\frac{\mathrm{d}h'}{\mathrm{d}\chi}+1\right)\right], \tag{25}$$

$$\frac{\mathrm{d}i'}{\mathrm{d}\chi} = 2\gamma_2\lambda\chi^{-1}\frac{\mathrm{d}}{\mathrm{d}\chi}\left[\frac{i'}{h'(\lambda-1)+1}\left(2\Gamma(h'-1)\chi\frac{\mathrm{d}h'}{\mathrm{d}\chi}+1\right)\right]. \tag{26}$$

Equations (25) and (26) are subject to the same conditions as listed in the previous section for the unknown $h'(\chi)$and $i'(\chi)$, which are equations (23) and (24), together with the conditions that there exists $\chi_{0,h}$ and $\chi_{0,i}$ where $h'(\chi_{0,h}) = 0$ and $i'(\chi_{0,i}) = 0$.

Evaluating (26) at $\chi_{0,i}$, we see that a non-zero derivative $\mathrm{d}i'/\mathrm{d}\chi$ can exist only when

$$1 = \frac{2\gamma_2\lambda}{h'(\lambda-1)+1}\left[2\Gamma(h'-1)\frac{\mathrm{d}h'}{\mathrm{d}\chi}+\frac{1}{\chi}\right]. \tag{27}$$

Therefore, (27) yields the point $\chi_{0,i}$, which is the minimum value of χ for which $i' = 0$. The equation set (25)–(26) may be solved sequentially for the two fronts, $h'(\chi)$ and $i'(\chi)$, where an analogous iterative method to that employed for finding h' can be used for i'. When $\Gamma = 0$, we can obtain an explicit expression for h' and i', similar to (14):

$$h' = \frac{1}{(\lambda-1)}\left(\sqrt{\frac{2\lambda\gamma_1}{\chi}}-1\right), \quad i' = c\left(\gamma_2\sqrt{\frac{2\lambda}{\gamma_1\chi}}-1\right), \tag{28}$$

where the integration constant c can be evaluated by (24) or (27),

$$c = \left(\lambda\frac{\gamma_2}{\gamma_1}-\gamma_1\right)^{-1}.$$

Aquifer thickness	15 m
Aquifer permeability	20 mD
Aquifer porosity	0.15
CO_2 viscosity	0.061 mPa s
Water viscosity	0.511 mPa s
CO_2 density	733 kg m^{-3}
Water density	1099 kg m^{-3}
Injected volume	1.2×10^6 m^3

TABLE 1. Problem set-up and relevant parameters for the injection problem example case.

We recall from the discussion following (14) that the expression for h' is valid for $\lambda > 1$. Similarly, as the mass transfer factor γ_2 approaches γ_1^2/λ from above, the expression for i' approaches a step function. For $\gamma_2 \leqslant \gamma_1^2/\lambda$, a piecewise constant solution satisfying (24) should be applied.

4. Results

To show how the solutions behave over a range of parameters, we consider solutions to a problem of constant injection of CO_2 into a saline aquifer, with both brine and CO_2 having constant properties. We first run a set of test problems that are also solved with a commercial numerical simulator, and compare the similarity solutions to full numerical solutions of the same problem. We then examine how the similarity solution behaves over a range of dimensionless parameter values, to show solution dependence on the key dimensionless parameters in the system. Finally, we examine the vertical equilibrium assumption over a range of flow conditions, to assess its applicability to the problem of carbon dioxide injection and transport.

The problem set-up is shown in figure 1, and relevant parameters for the injection problem are given in table 1. The problem corresponds to injection into a deep cold formation as identified in Nordbotten *et al.* (2005*b*), for which fluid properties are defined based on a typical hydrostatic pressure gradient of 10.5 MPa km^{-1}, and geothermal gradient of 25 K km^{-1}, resulting in temperature and pressure in the formation of 85°C and 31.5 MPa. Rock properties are taken to correspond to typical sedimentary formations in the Alberta Basin, as used previously by Nordbotten *et al.* (2005*a*, *b*). Injection rates are varied to span a range of practical injection rates, and to cover a corresponding reasonable set of values for the dimensionless parameter Γ. The injection rates range from a 'medium' injection rate of 120 m^3/day, which yields a relatively small value for Γ of 0.143, to 'low' (12 m^3/day) and then 'very low' (1.7 m^3/day) injection rates, corresponding to Γ values of 1.43 and 10, respectively. The total injected volume is chosen to be equivalent to 10 000 days (approximately 27 years) of operation for the medium injection rate. For comparison purposes, we also solve the same problem using the commercial multi-phase numerical simulator Eclipse (Schlumberger 2004). That code solves the full set of coupled multi-phase flow equations, using control volume discretizations in space and a fully implicit time-stepping scheme, and is widely considered the industry standard in petroleum engineering. For comparison purposes, we have programmed the numerical simulator in a black-oil formulation to ignore capillary pressure, and to use linear relative permeability functions. For the examples here, we have used a radially symmetric mode of Eclipse with logarithmic grid spacing, and we have used the vertically averaged volume fraction to compare to the similarity solutions presented above.

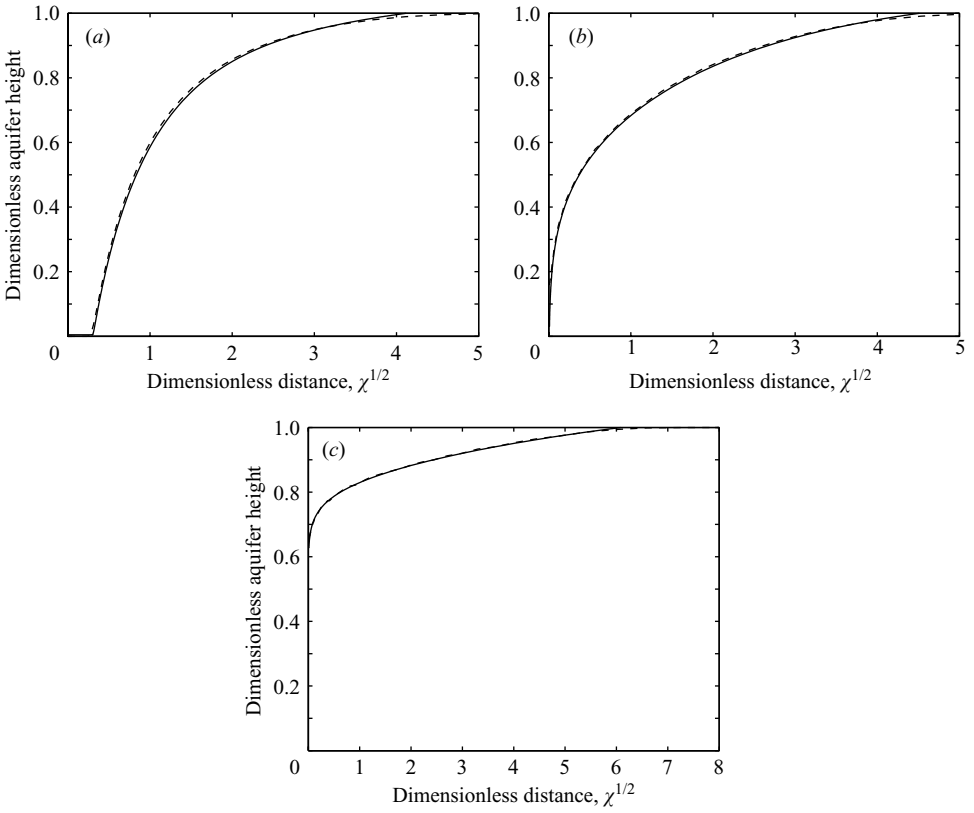

FIGURE 2. Comparison between a numerical solution (dashed line) and the similarity solution for (*a*) an intermediate injection rate, (*b*) a low injection rate, and (*c*) a very low injection rate.

To investigate the possibility of non-radial behaviour due to the invasion of a less viscous fluid into a more viscous fluid, we have also conducted full three-dimensional simulations on Cartesian grids for a range of parameters relevant to CO_2 injection. All our results indicate that even when the solution is perturbed, for example by introduction of a leaky abandoned well within the domain, radial symmetry is restored in the three-dimensional simulations.

Figure 2 shows results for the three different cases. Figure 2(*a*) shows results from the medium injection rate, corresponding to $\Gamma = 0.143$. In this case, viscous forces dominate the displacement process (Nordbotten *et al.* 2005*b*), so that the solution is very close to the analytical expression given in (14) for the case where Γ is negligibly small. Figure 2(*b*) uses a lower injection rate ($\Gamma = 1.43$), while figure 2(*c*) corresponds to a very low injection rate and the associated large value of $\Gamma = 10$. These results show that the similarity solutions capture the dominant displacement processes well, and the comparison to the results from Eclipse show excellent agreement across the full range of Γ values. Note that the Eclipse curves plotted in these figures are based on vertical integration of the numerically calculated saturations, and subsequent definition of an effective thickness of the CO_2 plume based on complete filling of the top-most part of the domain (residual saturation is set equal to zero in these calculations). This is similar to the way the solutions were used in Nordbotten *et al.* (2005*a*, *b*), and is consistent with an assumption of a sharp interface.

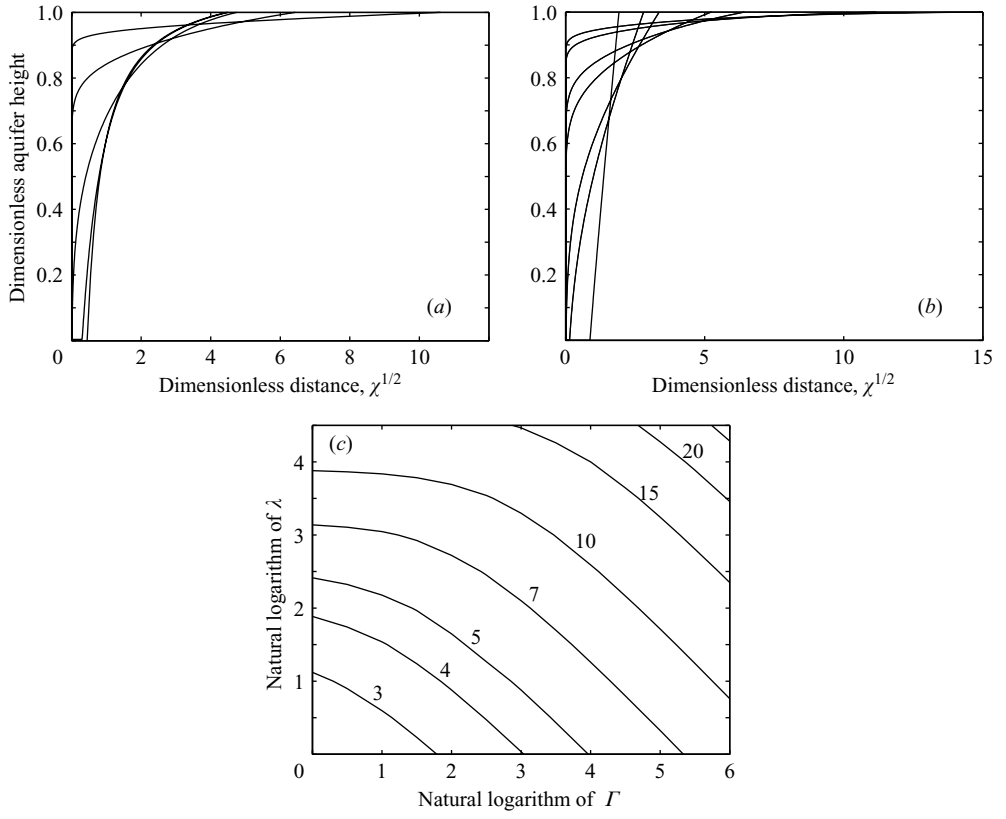

FIGURE 3. (*a*) Dependence of the incompressible similarity solution on the density parameter Γ. The curves range from $\Gamma = 0$ (closest to vertical) to $\Gamma = 100$ (closest to horizontal). $\lambda = 10$. (*b*) Dependence of the incompressible similarity solution on the viscosity ratio λ. The curves range from $\lambda = 0.1$ (closest to vertical) to $\lambda = 100$ (closest to horizontal). $\Gamma = 10$. (*c*) Dependence of the outer limit $\chi_{0,h}$ (shown as contour lines) of the incompressible similarity solution on the dimensionless gravity factor Γ and the viscosity ratio λ.

The next results show more general behaviour patterns in the similarity solutions, by spanning a range of parameter values for both the dimensionless parameter Γ and the mobility ratio λ. Figure 3(*a*) shows the family of curves for a fixed value of $\lambda = 10$, with Γ ranging from 0 to 100. These results show that there is little difference between the solutions for $\Gamma = 0$ and $\Gamma = 0.1$; the $\Gamma = 0$ solution is obtained from (14), while the solution with $\Gamma = 0.1$ is the full similarity solution corresponding to (13). The similarity solution begins to deviate from the viscous solution when $\Gamma = 1$, and is significantly different for larger values. So the range where the viscous solution is applicable corresponds to Γ values less than 1. Notice that in these results we interpret the '$\Gamma = 0$' case to mean that Γ is negligibly small, but that a density difference still exists (as it always does in the case of CO_2 injection into brine) and that vertical segregation of the fluids takes place owing to this density difference. Therefore the limit of small Γ should be interpreted as the limit of high injection rates. For the special case of equal densities, no gravity override occurs, and the interface position may be interpreted as representative of the vertically and angularly averaged fluid content, rather than a physical location of the interface position. This represents viscous instabilities in the absence of vertical segregation.

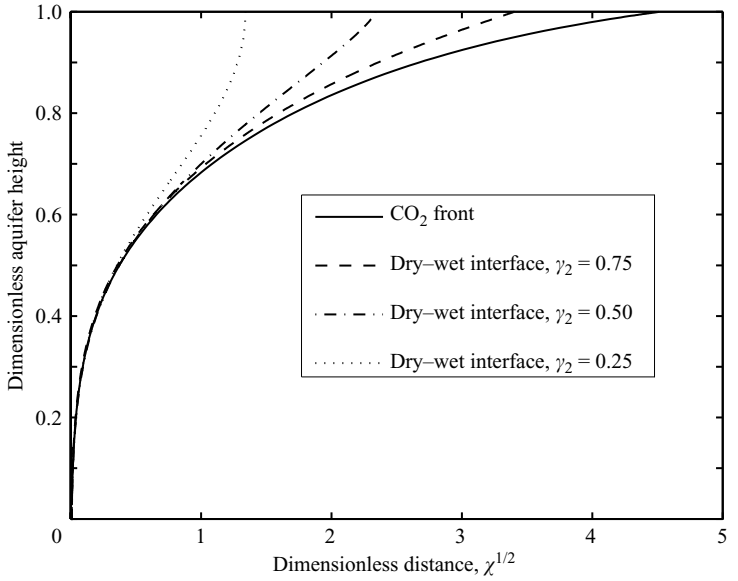

FIGURE 4. Dependence of the incompressible miscible similarity solution on the retardation parameter γ_2.

In figure 3(b), the value of Γ is fixed at 10, and the mobility ratio λ is varied from 0.1 to 100. For the highest values, which correspond to the most unfavourable ratios, the injected CO_2 forms a relatively thin layer at the top of the domain, showing the combined effect of gravity segregation and strong mobility contrast. These correspond to the plumes that spread farthest in space. Conversely, for strongly stable displacements, the profile becomes much more uniform in the vertical, approaching radial piston displacement as λ becomes small. The dependence of the extent of the plume (given by the variable $\chi_{0,h}$) on Γ and λ is summarized in figure 3(c). For the range of values investigated, we see that plume extent is more dependent on the mobility ratio λ than on the density parameter Γ.

The next result, in figure 4, shows how a drying front develops, when both wet and dry CO_2 are included in the analysis under the assumptions necessary for (25) and (26). The residual saturations and partitioning fractions are chosen such that γ_2 ranges from 0.25 to 0.75, while $\gamma_1 = 1$. An example leading to $\gamma_2 = 0.5$ has the residual saturation set to $S_{res} = 0.09$ and the partitioning fraction set to $\beta_2 = 0.1$. Figure 4 indicates that the original invasion front and the drying front are almost identical for small values of χ. However, at larger values of χ, a clear distinction between the two can be seen. The fraction of CO_2 volume that is 'wet' is relatively large, in these cases ranging from 75 % for the pair $\gamma_1 = 1$ and $\gamma_2 = 0.25$, to 25 % for the pair $\gamma_1 = 1$ and $\gamma_2 = 0.75$. The amount of CO_2 actually dissolved in the water phase will be a function of the residual saturation as well as the partitioning parameters and the gravity (Γ) and mobility (λ) parameters.

Finally, we consider calculations to demonstrate the importance of vertical flow, which allows for examination of the assumption of vertical equilibrium. This assumption is discussed in more detail in Appendix D. Figure 5(a) gives several numerical (Eclipse) solutions, corresponding to cases with different values of vertical permeability, plotted at different simulation times. The figure also shows one similarity solution, which coincides with the curve labelled '$k_z > 20$ mD'. All the curves in

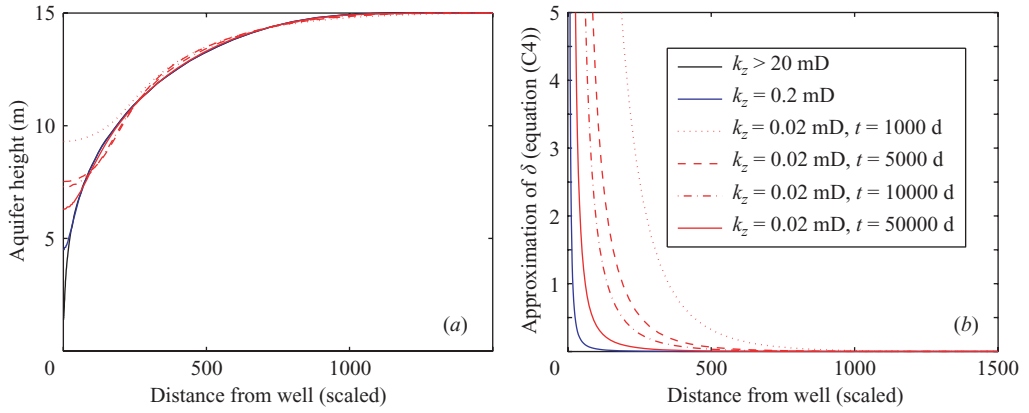

FIGURE 5. (*a*) Comparison between numerical solutions and the similarity solution for cases of a low injection rate. The different numerical solutions show the effect of vertical non-equilibrium. The curves for $k_z > 20$ mD, $k_z = 0.2$ mD are after 50 000 days of injection at the low injection rate, giving total injection volume of 6×10^5 m^3. The remaining curves are plotted scaled to an identical volume of CO_2 for comparison. (*b*) Estimate of the parameter δ based on (C 4) for the cases in (*a*). For comparision, the curves are plotted scaled to an identical volume of CO_2 as in (*a*). The curve for $k_z > 20$ mD is not visible on the plot since it is orders of magnitude smaller than the other curves.

the figure are scaled to have identical volumes of injected CO_2, corresponding to the amount injected in 1000 days at the rate used in figure 2(*b*). The horizontal permeability is 20 mD, so the anisotropy ratio varies from 1 to 1000. The case with the highest permeability anisotropy is shown in a time series, to assess the observations following equation (D 4) regarding the improvement of the vertical equilibrium assumption with time. The right-hand side of (D 4) is plotted in figure 5(*b*), which indicates, together with visual inspection of figure 5(*a*), that for $\delta(r, t)$ values below approximately one, the numerical solution lies close to the similarity solution. This indicates that the parameter δ provides a reasonable guideline for the applicability of the vertical equilibrium approximation. This is also consistent with the general idea of 'shallow' flow systems discussed in Huppert & Woods (1995), in that as the plume expands and the horizontal length scale increases, the shallow-flow assumption becomes progressively better for this system.

5. Conclusions

The solutions presented herein allow fluid interfaces to be computed across a range of injection conditions, for two-fluid flows under confined aquifer conditions. We have focused on conditions relevant for injection of CO_2 into deep, confined saline aquifers. For those systems, the injected fluid is always less dense and less viscous than the resident fluid. The general solutions capture the system behaviour well. In the limit of viscous domination, the general solution reduces to a simplified solution corresponding to the solution proposed by Nordbotten *et al.* (2005*b*) for practical CO_2 injection scenarios. The present solutions allow for residual saturations, mass transfer between the two fluids, and development of a drying front behind the main injection front. Fluid compressibility can also be included in the solutions, although all results presented in this paper use an assumption of constant fluid properties. A heuristic analysis provides guidelines to estimate the limit of significant vertical fluxes, such that the assumption of vertical equilibrium can be quantitatively evaluated.

Within the constraints of the vertical equilibrium assumption, and the assumption of a homogeneous, horizontal and confined aquifer, the solution presented herein is relatively general. The applicability of the solutions to problems of CO_2 injection is demonstrated through comparisons to numerical simulations, which show that the solutions represent the flow dynamics well. The solutions derived herein can also be applied to other deep injection systems, including those involving injection of acid gas (Bachu & Gunter 2004) and deep disposal of hazardous wastes (Smith 1996).

This work was supported in part by BP and the Ford Motor Company through funding to the Carbon Mitigation Initiative at Princeton University. We thank the anonymous reviewers for their many helpful suggestions, which have led to significant improvements in the paper.

Appendix A. Intermediate asymptotic of equation (12)

We wish to investigate the behaviour of the solution $h'(\chi,\tau)$ of (12), in particular its deviation from the stationary solution $h'(\chi)$ of (13). For ease of presentation we will use the shorthand notation $h'(\chi,\tau)=h$ and $h'(\chi)=h_0$.

We will assume that the fluid interface is monotone, such that we have for all χ and τ

$$\frac{\partial h}{\partial \chi} < 0, \quad \frac{\partial h_0}{\partial \chi} < 0. \tag{A 1}$$

Define the function

$$\chi'(\chi) = h^{-1}(h_0(\chi)) \tag{A 2}$$

as the function relating points χ' and χ where the functions h and h_0 have equal values. Now define χ_m as any point where the difference between $\chi'(\chi)$ and χ attains a local maximum:

$$|\chi'(\chi_m) - \chi_m| = \max_{\chi} |\chi'(\chi) - \chi|. \tag{A 3}$$

Then for $0 < h(\chi'(\chi_m)) < 1$ and $0 < h_0(\chi_m) < 1$, we have the properties that

$$\left.\begin{aligned} &\left.\frac{\partial h}{\partial \chi}\right|_{\chi'(\chi_m)} = \left.\frac{\mathrm{d}h_0}{\mathrm{d}\chi}\right|_{\chi_m}, \quad \left.\frac{\mathrm{d}\chi'}{\mathrm{d}\chi}\right|_{\chi'(\chi_m)} = 1, \\ &\operatorname{sign}\left(\left.\frac{\partial^2 h}{\partial \chi^2}\right|_{\chi'(\chi_m)} - \left.\frac{\mathrm{d}^2 h_0}{\mathrm{d}\chi^2}\right|_{\chi_m}\right) = -\operatorname{sign}(\chi'(\chi_m) - \chi_m) \end{aligned}\right\} \tag{A 4}$$

Now, subtracting (13) from (12) we obtain

$$\begin{aligned} \tau \left.\frac{\partial h}{\partial \tau}\right|_{\chi'(\chi_m)} \left(\left.\frac{\mathrm{d}h_0}{\mathrm{d}\chi}\right|_{\chi_m}\right)^{-1} = [\chi'(\chi_m) - \chi_m] \Bigg[1 - \frac{4\Gamma\lambda^2 h_0(\chi_m)}{(1+(\lambda-1)h_0(\chi_m))^2} \left.\frac{\mathrm{d}h_0}{\mathrm{d}\chi}\right|_{\chi_m} \\ + \frac{4\Gamma\lambda(1-h_0(\chi_m))}{1+(\lambda-1)h_0(\chi_m)} \left.\frac{\mathrm{d}h_0}{\mathrm{d}\chi}\right|_{\chi_m}\Bigg] + \frac{4\Gamma\lambda h_0(\chi_m)(1-h_0(\chi_m))}{1+(\lambda-1)h_0(\chi_m)} \\ \times \left(\left.\frac{\mathrm{d}h_0}{\mathrm{d}\chi}\right|_{\chi_m}\right)^{-1} \left(\chi'(\chi_m) \left.\frac{\partial^2 h}{\partial \chi^2}\right|_{\chi'(\chi_m)} - \chi_m \left.\frac{\mathrm{d}^2 h_0}{\mathrm{d}\chi^2}\right|_{\chi_m}\right). \end{aligned} \tag{A 5}$$

This implies that

$$\left.\frac{\partial h}{\partial \tau}\right|_{\chi'(\chi_m)} \left(\left.\frac{\mathrm{d}h_0}{\mathrm{d}\chi}\right|_{\chi_m}\right)^{-1} = \frac{c_1}{\tau}[\chi'(\chi_m) - \chi_m] + \frac{c_2}{\tau}\left(\left.\frac{\partial^2 h}{\partial \chi^2}\right|_{\chi'(\chi_m)} - \left.\frac{\mathrm{d}^2 h_0}{\mathrm{d}\chi^2}\right|_{\chi_m}\right), \tag{A 6}$$

where the coefficients c_1 and c_2 are defined as

$$c_1 = 1 - \Gamma\left[\frac{4\lambda}{1+(\lambda-1)h_0(\chi_m)}\left(\frac{\lambda h_0(\chi_m)}{1+(\lambda-1)h_0(\chi_m)} - (1-h_0(\chi_m))\right)\left.\frac{\mathrm{d}h_0}{\mathrm{d}\chi}\right|_{\chi_m} - \frac{4\lambda h_0(\chi_m)(1-h_0(\chi_m))}{1+(\lambda-1)h_0(\chi_m)}\left(\left.\frac{\mathrm{d}h_0}{\mathrm{d}\chi}\right|_{\chi_m}\right)^{-1}\left.\frac{\mathrm{d}^2h_0}{\mathrm{d}\chi^2}\right|_{\chi_m}\right], \quad \text{(A 7}a\text{)}$$

$$c_2 = \chi'(\chi_m)\frac{4\Gamma\lambda h_0(\chi_m)(1-h_0(\chi_m))}{1+(\lambda-1)h_0(\chi_m)}\left(\left.\frac{\mathrm{d}h_0}{\mathrm{d}\chi}\right|_{\chi_m}\right)^{-1}. \quad \text{(A 7}b\text{)}$$

We see that if $\mathrm{d}h_0/\mathrm{d}\chi$ and $\mathrm{d}^2h_0/\mathrm{d}\chi^2$ are bounded, c_1 will be a positive coefficient when $\Gamma < \Gamma_{crit}$, for some value Γ_{crit} dependent on λ, and the properties of the stationary solution; h_0 and $\mathrm{d}h_0/\mathrm{d}\chi$. Also, c_2 will be negative under assumption (A 1). In the following derivation we will assume that Γ is below this critical value. We can now use inequalities (A 1) as well as properties (A 4) to obtain

$$\begin{aligned}\frac{\partial}{\partial\tau}(\chi'(\chi_m)-\chi_m) &= \left.\frac{\partial\chi'}{\partial\tau}\right|_{\chi_m} = -\left.\frac{\partial h}{\partial\tau}\right|_{\chi'(\chi_m)}\left(\left.\frac{\partial h_0}{\partial\chi}\right|_{\chi_m}\right)^{-1} \\ &= -\frac{c}{\tau}(\chi'(\chi_m)-\chi_m) - \frac{c_2}{\tau}\left(\left.\frac{\partial^2 h}{\partial\chi^2}\right|_{\chi'(\chi_m)} - \left.\frac{\mathrm{d}^2h_0}{\mathrm{d}\chi^2}\right|_{\chi_m}\right). \quad \text{(A 8)}\end{aligned}$$

From this equation and the last property of (A 4), we see that the maximum difference between the points χ' and χ is strictly decreasing when the maximum difference is not at the endpoints of the domain.

If χ_m is at the top boundary of the domain, then $h(\chi_m)=0$. We can again subtract (13) from (12) as we did above to obtain

$$\left.\frac{\partial h}{\partial\tau}\right|_{\chi'(\chi_m)}\left(\left.\frac{\mathrm{d}h_0}{\mathrm{d}\chi}\right|_{\chi_m}\right)^{-1} = \frac{1}{\tau}[\chi'(\chi_m)-\chi_m] + \frac{4\Gamma\lambda}{\tau}\left(\chi'(\chi_m)\left.\frac{\partial h}{\partial\chi}\right|_{\chi'(\chi_m)} - \chi_m\left.\frac{\mathrm{d}h_0}{\mathrm{d}\chi}\right|_{\chi_m}\right). \quad \text{(A 9)}$$

Since χ_m is a local maximum, sign $(\partial h/\partial\chi - \mathrm{d}h_0/\mathrm{d}\chi) = \mathrm{sign}(\chi'(\chi_m)-\chi_m)$. Thus the equivalent expression to (A 8) for the top boundary is

$$\left.\begin{aligned}\frac{\partial}{\partial\tau}\chi'(\chi_m) &> -\frac{1}{\tau}\left(1+4\Gamma\lambda\left.\frac{\mathrm{d}h_0}{\mathrm{d}\chi}\right|_{\chi_m}\right)[\chi'(\chi_m)-\chi_m] \quad \text{when} \quad \chi'(\chi_m) < \chi_m, \\ \frac{\partial}{\partial\tau}\chi'(\chi_m) &< -\frac{1}{\tau}\left(1+4\Gamma\lambda\left.\frac{\mathrm{d}h_0}{\mathrm{d}\chi}\right|_{\chi_m}\right)[\chi'(\chi_m)-\chi_m] \quad \text{when} \quad \chi'(\chi_m) > \chi_m.\end{aligned}\right\} \quad \text{(A 10)}$$

If χ_m is at the bottom boundary of the domain, then $h(\chi_m)=1$, and sign $(\partial h/\partial\chi - \mathrm{d}h_0/\mathrm{d}\chi) =$ sign$(\chi_m - \chi'(\chi_m))$. By the same arguments as for the top boundary, the equivalent expression to (A 8) for the bottom boundary is

$$\left.\begin{aligned}\frac{\partial}{\partial\tau}\chi'(\chi_m) &> -\frac{1}{\tau}\left(1-4\Gamma\left.\frac{\mathrm{d}h_0}{\mathrm{d}\chi}\right|_{\chi_m}\right)[\chi'(\chi_m)-\chi_m] \quad \text{when} \quad \chi'(\chi_m) < \chi_m, \\ \frac{\partial}{\partial\tau}\chi'(\chi_m) &< -\frac{1}{\tau}\left(1-4\Gamma\left.\frac{\mathrm{d}h_0}{\mathrm{d}\chi}\right|_{\chi_m}\right)[\chi'(\chi_m)-\chi_m] \quad \text{when} \quad \chi'(\chi_m) > \chi_m.\end{aligned}\right\} \quad \text{(A 11)}$$

From this we can conclude that for $\Gamma < \Gamma_{crit}$, all maxima of $|\chi' - \chi|$ must be strictly decreasing, independent of whether the maxima are internal or on the boundary.

In sum, we have shown that for sufficiently small Γ, dependent on λ, and h_0, equation (12) has the stable stationary solution given by (13). Equations (A 8), (A 10)

and (A 11) show that all local maxima of the function $|\chi' - \chi|$ must be decreasing, and we therefore have the conclusion that as τ goes to infinity the solution $h'(\chi,\tau)$, if it is monotone, will converge to $h'(\chi)$.

Appendix B. Derivation of mass transfer factors

In (18), we introduced the factors γ_1 and γ_2 representing the effects of mass transfer at the interface between water and wet CO_2 and the interface between wet CO_2 and dry CO_2, respectively. For completeness, we derive those factors in this Appendix.

Consider first the second mass transfer factor, γ_2, representing the relationship between flow of dry CO_2 and the movement of the interface between dry CO_2 and the composite region composed of wet CO_2 and residual brine. For this interface, we can write the following mass balance for CO_2:

$$\phi(v_c - v_I) = \phi(v_{cw} - v_I)(1 - S_{res})(1 - \beta_2) - \phi v_I S_{res}\beta_1. \tag{B 1}$$

Here, v_c and v_{cw} refer to the velocity of dry and wet CO_2, respectively, while v_I represents the velocity of the interface. The left-hand side of (B 1) refers to the mass flux of CO_2 in the dry CO_2 phase into the interface (interface $i(r,t)$ in figure 1). The first term on the right-hand side is the outflow of CO_2 carried by the wet CO_2 phase away from the interface, while the last term is CO_2 recovered from the evaporating saturated residual water. A similar balance can be written for the fluxes of water into and out of the interface $i(r,t)$, and this takes the following form,

$$0 = \phi(v_{cw} - v_I)(1 - S_{res})\beta_2 - \phi v_I S_{res}(1 - \beta_1). \tag{B 2}$$

Because there is no flux of water into the interface from the left side, the left-hand side of equation (B 2) is zero. The first term on the right-hand side represents outflow of water in the wet CO_2 phase, while the last term represents water evaporating into the CO_2 phase from the residual saturation. Combining these equations allows us to define the retardation factor γ_2 as used in (18). It takes the following form,

$$\gamma_2 = (1 - S_{res})\frac{v_I}{v_{cw}} = \left[1 + \frac{(1 - \beta_1)S_{res}}{(1 - S_{res})\beta_2}\right]^{-1}. \tag{B 3}$$

Similarly, for the first mass transfer factor, γ_1, representing the relationship between flow of water and the movement of the interface between water and the composite region, we have the mass conservation equation for the CO_2 phase

$$\phi(v_{cw} - v_I)(1 - S_{res})(1 - \beta_2) - \phi v_I S_{res}\beta_1 = 0, \tag{B 4}$$

where now v_I refers to the interface between water and the composite region. For the water phase, the analogous equation is

$$\phi(v_{cw} - v_I)(1 - S_{res})\beta_2 - \phi v_I S_{res}(1 - \beta_1) = \phi(v_w - v_I). \tag{B 5}$$

Combined, (B 4) and (B 5) give the following mass transfer factor

$$\gamma_1 = (1 - S_{res})\frac{v_I}{v_w} = \left[1 + \frac{\beta_1 S_{res}}{(1 - S_{res})(1 - \beta_2)}\right]^{-1}. \tag{B 6}$$

Appendix C. Pressure-dependent densities and viscosities

The analysis presented for the incompressible cases can be extended to the more general case of pressure-dependent densities and viscosities, although this

is significantly more complicated, and for many practical problems not necessary (Nordbotten *et al.* 2005*a*,*b*). The approach is analogous to the developments already presented, so in this section the corresponding generalizations of the earlier equations are presented, and the overall approach is briefly outlined.

To begin, the general equation for pressure distributions in the vertical may be written as

$$\begin{aligned} p(r,t,0) = p(r,t,H) &- \int_0^{i(r,t)} \left[\rho_c(p(r,t,z))g + \frac{q_{c,z}(r,t,z)\mu_c(p(r,t,z))}{k_z(r,z)}\right] \mathrm{d}z \\ &- \int_{i(r,t)}^{h(r,t)} \left[\rho_{cw}(p(r,t,z))g + \frac{q_{cw,z}(r,t,z)\mu_{cw}(p(r,t,z))}{k_z(r,z)}\right] \mathrm{d}z \\ &- \int_{h(r,t)}^{H} \left[\rho_w(p(r,t,z))g + \frac{q_{w,z}(r,t,z)\mu_w(p(r,t,z))}{k_z(r,z)}\right] \mathrm{d}z. \end{aligned} \tag{C 1}$$

In (C 1), the pressure dependence of the density and viscosity are noted explicitly. The assumption of vertical equilibrium, which is appropriate when the changes in pressure in the vertical owing to vertical flow are small compared to the density contributions, and are small compared to horizontal flow components, allows (C 2) to be simplified as

$$\begin{aligned} p(r,t,0) = p(r,t,H) &- \int_0^{i(r,t)} \rho_c(p(r,t,z))g \,\mathrm{d}z \\ &- \int_{i(r,t)}^{h(r,t)} \rho_{cw}(p(r,t,z))g \,\mathrm{d}z - \int_{h(r,t)}^{H} \rho_w(p(r,t,z))g \,\mathrm{d}z. \end{aligned} \tag{C 2}$$

This implies that if, for example, the bottom pressure $p_H(r,t) = p(r,t,H)$ is known for all r, then the pressure is known everywhere, once i and h are known. We therefore take

$$p(r,t,z) = p(p_H(r,t), i(r,t), h(r,t), z), \tag{C 3}$$

as a given function.

Given the assumptions of vertical equilibrium and radial symmetry about the injection well, the mass flows of the three fluids through a cylindrical surface at an arbitrary radius r may be written as

$$\left.\begin{aligned} Q_w(r,t) &= -2\pi r \int_{h(r,t)}^{H} \rho_w(p(r,t,z)) \frac{k_r(z)}{\mu_w(p(r,t,z))} \frac{\partial}{\partial r} p(r,t,z) \,\mathrm{d}z, \\ Q_{cw}(r,t) &= -2\pi r \int_{i(r,t)}^{h(r,t)} \rho_{cw}(p(r,t,z)) \frac{k_r(z)}{\mu_{cw}(p(r,t,z))} \frac{\partial}{\partial r} p(r,t,z) \,\mathrm{d}z, \\ Q_c(r,t) &= -2\pi r \int_{0}^{i(r,t)} \rho_c(p(r,t,z)) \frac{k_r(z)}{\mu_c(p(r,t,z))} \frac{\partial}{\partial r} p(r,t,z) \,\mathrm{d}z. \end{aligned}\right\} \tag{C 4}$$

Given further the assumptions of essentially horizontal flow, the existence of residual saturation in the wet CO_2 region, and the dissolution of CO_2 into the residual water

in the wet CO_2 zone, a mass balance statement can be written for each of the three regions. The form of these equations is as follows,

$$\left.\begin{aligned}
\frac{\partial}{\partial t}\int_{h(r,t)}^{H}\varphi\rho_w \mathrm{d}z &= \frac{-\gamma_1}{(1-S_{res})2\pi r}\frac{\partial}{\partial r}Q_w(r,t),\\
\frac{\partial}{\partial t}\int_{i(r,t)}^{h(r,t)}\varphi\rho_{cw}\mathrm{d}z &= \frac{-1}{(1-S_{res})2\pi r}\frac{\partial}{\partial r}Q_{cw}(r,t)-\frac{1-\gamma_2}{2\pi r}\frac{\partial}{\partial r}Q_c(r,t)\\
&\quad -\frac{1-\gamma_1}{(1-S_{res})2\pi r}\frac{\partial}{\partial r}Q_w(r,t),\\
\frac{\partial}{\partial t}\int_{0}^{i(r,t)}\varphi\rho_c \mathrm{d}z &= \frac{-\gamma_2}{2\pi r}\frac{\partial}{\partial r}Q_c(r,t).
\end{aligned}\right\} \tag{C 5}$$

These equations have a stationary solution in the similarity variable $\xi = r^2/t$:

$$\left.\begin{aligned}
Q_w(\xi) &= -4\pi\xi\int_{h(\xi)}^{H}\rho_w(p(\xi,z))\frac{k_r(z)}{\mu_w(p(\xi,t))}\frac{\partial}{\partial\xi}p(\xi,z)\,\mathrm{d}z,\\
Q_c(\xi) &= -4\pi\xi\int_{0}^{i(\xi)}\rho_c(p(\xi,z))\frac{k_r(z)}{\mu_c(p(\xi,t))}\frac{\partial}{\partial\xi}p(\xi,z)\,\mathrm{d}z,\\
Q_{cw}(\xi) &= -4\pi\xi\int_{i(\xi)}^{h(\xi)}\rho_{cw}(p(\xi,z))\frac{k_r(z)}{\mu_{cw}(p(\xi,t))}\frac{\partial}{\partial\xi}p(\xi,z)\,\mathrm{d}z,
\end{aligned}\right\} \tag{C 6}$$

and

$$\left.\begin{aligned}
\frac{\partial}{\partial\xi}\int_{h(\xi)}^{H}\varphi\rho_w(p(\xi,z))\,\mathrm{d}z &= \frac{-\gamma_1}{(1-S_{res})\pi\xi}\frac{\partial}{\partial\xi}Q_w(\xi),\\
\frac{\partial}{\partial\xi}\int_{i(\xi)}^{h(\xi)}\varphi\rho_{cw}(p(\xi,z))\,\mathrm{d}z &= \frac{-1}{(1-S_{res})\pi\xi}\frac{\partial}{\partial\xi}Q_{cw}(\xi)-\frac{1-\gamma_2}{\pi\xi}\frac{\partial}{\partial\xi}Q_c(\xi)\\
&\quad -\frac{1-\gamma_1}{(1-S_{res})\pi\xi}\frac{\partial}{\partial\xi}Q_w(\xi),\\
\frac{\partial}{\partial\xi}\int_{0}^{i(\xi)}\varphi\rho_c(p(\xi,z))\,\mathrm{d}z &= \frac{-\gamma_2}{\pi\xi}\frac{\partial}{\partial\xi}Q_c(\xi).
\end{aligned}\right\} \tag{C 7}$$

Equations (C 6) and (C 7) together with (C 3) form a system of six first-order ordinary differential equations for the dependent variables Q_c, Q_{cw}, Q_w, p, i and h, thus showing that the full equations exhibit self-similar solutions given the vertical equilibrium assumption and appropriate boundary conditions. The boundary conditions that satisfy the scaling $\xi = r^2/t$ are as in the preceding cases, apart from all volume balances being replace by mass balance, based on a constant mass injection rate.

Solving this system of equations is more involved than those in §§ 3.1 and 3.2, since the pressure solution will feed back into fluid properties. We propose the following iterative solution technique:

0. Use the solution to (20) as an initial guess, with pressure given by the initial pressure.

1. Update the fluid properties (density and viscosity) corresponding to the pressure solution from the previous iteration.

2. Solve (C 7) numerically, holding the updated fluid properties constant.

3. Repeat from step 1 until converged.

Appendix D. Vertical equilibrium

The assumption of vertical equilibrium can be analysed *a posteriori*. We will present the arguments for this in the setting of the incompressible case without mass transfer above, to keep the notation simple. Let $\delta(r,t)$ be a measure of the error introduced by the vertical equilibrium assumption,

$$\delta(r,t) = \frac{p(r,t,0) - p_{ex}(r,t,0)}{p(r,t,H) - p(r,t,0)}, \tag{D 1}$$

where subscript *ex* denotes the top pressure obtained by application of (1) to a given flow field and bottom pressure, while p without subscript indicates the pressure obtained from (2).

The numerator of (D 1) can be estimated from the flow fields implied from the interface. For a given depth z_0, the fluid injected below z_0 must exceed the total vertical flux inside the plume at this depth unless the plume contracts at some height,

$$\frac{H - z_0}{H} Q_{well} \geqslant q_{c,z} \pi r^2(z_0,t). \tag{D 2}$$

Here, $r(z_0,t)$ is the radius of the plume at a given depth, which is obtained by inverting the function $h(r,t)$, and $q_{c,z}$ is interpreted as the horizontally averaged vertical flux inside the plume. Inequality (D 2) can be used to approximate the first integral in (1), which on substitution into (D 1) gives

$$\delta(z_0,t) \leqslant \frac{Q_{well}(H - z_0)z_0}{\pi r^2(z_0,t)H} \frac{\mu_c}{k_z k_{r,c}} \frac{1}{\rho_c g z_0 + \rho_w g(H - z_0)}. \tag{D 3}$$

This can be reformulated using radius r as a primary variable,

$$\delta(r,t) \leqslant \frac{Q_{well}(H - h(r,t))h(r,t)}{\pi r^2 H} \frac{\mu_c}{k_z k_{r,c}} \frac{1}{\rho_c g h(r,t) + \rho_w g(H - h(r,t))}. \tag{D 4}$$

This expression for $\delta(r,t)$ is based on several approximations, and should be considered as an indicator of the importance of vertical disequilibrium, rather than a rigid justification for the application of vertical equilibrium. Acceptable values for $\delta(r,t)$ are discussed in § 4.

By inspection of (D 4), we see that for a fixed radius, $\delta(r,t)$ is a decreasing function of time, since $h(r,t)$ is an increasing function bounded above by H. This implies that the validity of the vertical equilibrium assumption increases with time, and thus we may expect the similarity solution to more closely mimic the true solution for late times. Similarly, we see that the vertical permeability appears in the denominator of (D 4); thus as expected, the vertical equilibrium assumption is most applicable when the vertical permeability is not too low.

REFERENCES

Bachu, S. 2003 Screening and ranking of sedimentary basins for sequestration of CO_2 in geological media. *Environ. Geol.* **44**, 277–289.

Bachu, S. & Gunter, W. D. 2004 Acid gas injection in the Alberta basin, Canada: a CO_2 storage experience. In *Geological Storage of Carbon Dioxide for Emissions Reduction: Technology* (ed. S. J. Baines & R. H. Worden), p. 225–234, Geological Society Special Publication, Bath, UK, SP 233.

Barenblatt, G. I. 1990 *Theory of Fluid Flows through Natural Rocks*. Kluwer.

Barenblatt, G. I. 1996 *Scaling, Self-Similarity, and Intermediate Asymptotics*. Cambridge University Press.

Bear, J. 1979 *Hydraulic of Groundwater*. McGraw–Hill.

Blunt, M. & King, P. 1991 Relative permeabilities from two- and three-phase pore-scale network modeling. *Transp. Porous Media* **6,** 407–433.

Bruant, R. G., Guswa, A. J., Celia, M.A. & Peters, C. A. 2002 Safe storage of carbon dioxide in deep saline aquifers. *Environ. Sci. Technolo*, 1 June, 241A–245A.

Dullien, F. A. L. 1992 *Porous Media: Fluid Transport and Pore Structure*. Academic.

Donaldson, E. C. 1964 *Subsurface disposal of industrial waste in the United States, US Bur. Mines Inf. Circ.* 8212, 32 pp.

Enick, R. M. & Klara, S. M. 1990 CO_2 solubility in water and brine under reservoir conditions. *Chem. Engng Commun.* **90**, 23–33.

Holloway, S., Chadwick, A., Lindeberg, E., Czernichowski-Lauriol, I. & Arts, R. 2004 *Best Practice Manual from SACS Saline Aquifer Storage Project*. Statoil, Trondheim, Norway.

Huppert, H. E. & Woods, A. W. 1995 Gravity driven flows in porous layers. *J. Fluid Mech.* **292**, 55–69.

Jupp, T. E. & Woods, A. W. 2003 Thermally driven reaction fronts in porous media. *J. Fluid Mech.* **484,** 329–346.

King, S. E. & Woods, A. W. 2003 Dipole solutions for viscous gravity currents: theory and experiments. *J. Fluid Mech.* **483**, 91–109.

Nordbotten, J. M., Celia, M. A. & Bachu, S. 2004 Analytical solutions for leakage rates through abandoned wells. *Wat. Resour. Res.* **40**(4), W04204, doi:10.1029/2003WR002997.

Nordbotten, J. M., Celia, M. A., Bachu, S. & Dahle, H. K. 2005*a* Semi-analytical solution for CO_2 leakage through an abandoned well. *Environ. Sci. Technol.* **39**, 602–611.

Nordbotten, J. M., Celia, M. A. & Bachu, S. 2005*b* Injection and storage of CO_2 in deep saline aquifers: analytical solution for CO_2 plume evolution during injection. *Transp. Porous Media* **55**, 339–360.

Pacala, S. & Socolow, R. 2004 Stabilization wedges: solving the climate problem for the next 50 years with current technologies. *Science* **305**, 968–972.

Raw, A. W. V. & Woods, A. W. 2003 On gravity-driven flow through a reacting porous rock. *J. Fluid Mech.* **474**, 227–243.

Schlumberger Information Systems 2004 *Eclipse Technical Description.*

Smith, R. E. 1996 EPA mission research in support of hazardous waste injection 1986–1994. In *Deep Injection Disposal of Hazardous and Industrial Waste* (ed. J. A. Apps & C.-F. Tsang), pp. 9–24. Academic.

Torp, T. A. & Gale, J. 2004 Demonstrating storage of CO_2 in geological reservoirs: the Sleipner SACS project. *Energy* **29**, 1361–1369.

US Environmental Protection Agency 1985 Report to congress on injection of hazardous waste, *EPA 570/9-85-003*, Office of Drinking Water, Washington, DC.

Woods, A. W. & Mason, R. 2000 The dynamics of two-layer gravity-driven flows in permeable rock. *J. Fluid Mech.* **421**, 83–114.